nature physics

Article

https://doi.org/10.1038/s41567-023-02091-7

Anderson localization of electromagnetic waves in three dimensions

Received: 6 September 2022

Accepted: 11 May 2023

Published online: 15 June 2023

Check for updates

Alexey Yamilov [1] ✉, Sergey E. Skipetrov [2], Tyler W. Hughes[3], Momchil Minkov[3], Zongfu Yu [4] ✉ & Hui Cao [5] ✉

Anderson localization is a halt of diffusive wave propagation in disordered systems. Despite extensive studies over the past 40 years, Anderson localization of light in three dimensions has remained elusive, leading to the question of its very existence. Recent advances have enabled finite-difference time-domain calculations to be sped up by orders of magnitude, allowing us to conduct brute-force numerical simulations of light transport in fully disordered three-dimensional systems with unprecedented dimension and refractive index difference. We show numerically three-dimensional localization of vector electromagnetic waves in random aggregates of overlapping metallic spheres, in sharp contrast to the absence of localization for dielectric spheres with a refractive index up to 10 in air. Our work opens a wide range of avenues in both fundamental research related to Anderson localization and potential applications using three-dimensional localized light.

Anderson localization (AL)[1] is an emergent phenomenon for both quantum and classical waves including electron[2–4], cold-atom[5,6], electromagnetic (EM)[7–11], acoustic[12,13], water[14], seismic[15] and gravity[16] waves. Unlike in one or two dimensions, AL in three dimensions requires strong disorder[1,17–19]. A mobility edge separating the diffuse transport regime from AL can be estimated from the Ioffe–Regel criterion $k_{\mathrm{eff}}\ell_s \approx 1$, where k_{eff} is the effective wavenumber in the medium and ℓ_s is the scattering mean free path[20]. This criterion suggests two avenues to achieving localization: reduction of k_{eff} or ℓ_s. For EM waves, the reduction of k_{eff} is realized by introducing partial order or spatial correlation in the position of scatterers[7,21]. In comparison, reaching localization of light in fully random photonic media by increasing the scattering strength (decreasing ℓ_s) turns out to be much more challenging[22,23]. Despite successful experiments in low-dimensional systems[9,10,24], three-dimensional (3D) localization remained stubbornly elusive[25], which triggered theoretical[26,27] and experimental[28] studies of the mechanisms that impede it.

Anderson himself originally proposed "a system composed essentially of random waveguides near cut-off and random resonators, such as might be realized by a random packing of metallic balls of the right size" as "the ideal system" for localization of EM radiation[8]. In practice, the absorption of metals obscures localization[9,29], and the experimental focus shifted to dielectric materials with low loss and high refractive index[29–33]. However, even for dielectric systems, experimental artefacts due to residual absorption and inelastic scattering mar the data[22,23,34–36]. Numerically, these artefacts can be excluded, but 3D random systems of sufficiently large dimension and large refractive index variation could not be simulated due to an extraordinarily long computational time required[37,38].

A recent implementation of the finite-difference time-domain (FDTD) algorithm on emerging computing hardware has brought orders of magnitude speed-up of numerical calculation[39,40]. Using this highly efficient hardware-optimized version of the FDTD method, we solve the Maxwell equations by brute force in three dimensions. This enables us to simulate sufficiently large systems and large refractive index variation to address the following questions: can 3D AL of EM waves be achieved in fully random systems of dielectric scatterers? If not, can it occur in any other systems without the aid of spatial correlations?

Answering these long-standing questions not only addresses the fundamental aspects of wave transport and localization across multiple

[1]Physics Department, Missouri University of Science and Technology, Rolla, MO, USA. [2]Univ. Grenoble Alpes, CNRS, LPMMC, Grenoble, France. [3]Flexcompute Inc, Belmont, MA, USA. [4]Department of Electrical and Computer Engineering, University of Wisconsin, Madison, WI, USA. [5]Department of Applied Physics, Yale University, New Haven, CT, USA. ✉e-mail: yamilov@mst.edu; zyu54@wisc.edu; hui.cao@yale.edu

https://doi.org/10.1038/s41567-023-02091-7

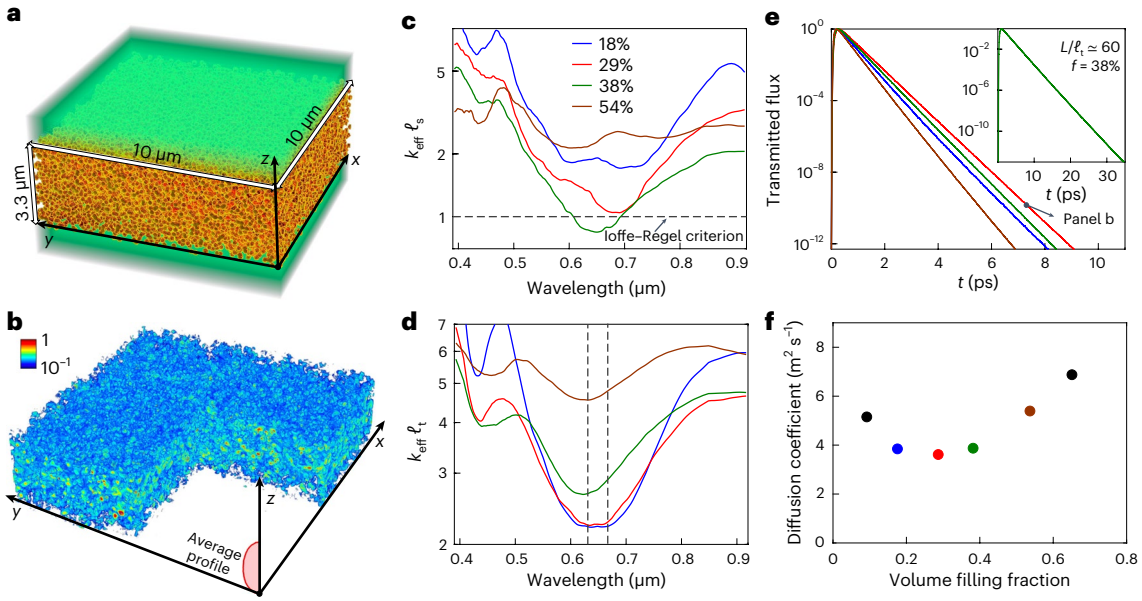

Fig. 1 | Absence of non-diffusive transport in random dielectric systems with a refractive index of 3.5. a, A 3D slab filled with dielectric spheres at random uncorrelated positions (radius $r = 100$ nm, refractive index $n = 3.5$) in air. The slab cross-section is 10 μm × 10 μm = 100 μm², and the thickness is $L = 3.3$ μm. **b**, The 3D distribution of light intensity inside the slab (dielectric filling fraction $f = 29\%$, $L/\ell_t = 33$) at long delay time after a short pulse of plane wavefront is incident on the front surface. The red curve with shading shows the average depth profile. **c**, The spectral dependence of the Ioffe–Regel parameter $k_{\text{eff}}\ell_s$ for different volume filling fractions of dielectric spheres, showing enhancement of scattering around single-sphere Mie resonances. The horizontal dashed line marks the Ioffe–Regel criterion $k_{\text{eff}}\ell_s = 1$ for 3D localization. **d**, The transport mean free path ℓ_t (in units of $1/k_{\text{eff}}$) as a function of wavelength, revealing a saturation by dependent scattering at high dielectric filling fractions. The vertical dashed lines mark the spectral width (33 nm) of the excitation pulse in **b** and **e**. **e**, Transmittance of the 3D slab for a pulsed excitation, showing exponential decay in time for all dielectric filling fractions, in agreement with diffusive transport. The inset shows persistence of diffusion when L/ℓ_t is increased from 33 to 60 for $f = 38\%$ (green line). **f**, The dependence of the minimum diffusion coefficient within the pulse bandwidth on the dielectric filling fraction f, exhibiting a minimum value of 3.6 $m^2\,s^{-1}$ at $f \approx 30\%$.

disciplines but also opens new avenues in research and applications. For example, in topological photonics[41], the interplay between disorder and topological phenomena may be explored beyond the limit of weak disorder in low-dimensional systems[42]. Also in cavity quantum electrodynamics with Anderson-localized modes[43], achieving 3D localization would avoid the out-of-plane loss inherent to two-dimensional (2D) systems and cover the full angular range of propagation directions[44]. In addition to fundamental studies, disorder and scattering has been harnessed for various photonic device applications, but mostly with diffuse waves[45]. Anderson-localized modes can be used for 3D energy confinement to enhance optical non-linearities and light–matter interactions, and to control random lasing as well as targeted energy deposition.

We first consider EM wave propagation through a 3D slab of randomly packed lossless dielectric spheres of radius $r = 100$ nm and refractive index $n = 3.5$ in air. This corresponds to the highest index difference achieved experimentally in the optical wavelength range with porous GaP around the wavelength of $\lambda = 650$ nm in the vicinity of the first Mie resonance of an isolated sphere (Supplementary Fig. S5). To avoid spatial correlations, the sphere positions are chosen completely randomly, leading to spatial overlap where the index is capped at the same value of n. We compute the spatial correlation function of such structure, which reveals that the correlation vanishes beyond the particle diameter (Supplementary Fig. S4). To avoid light reflection at the interfaces of the slab, we surround it by a uniform medium with a refractive index equal to the effective index of the slab, $n_{\text{eff}} = [(1-f) + fn^2]^{1/2}$, for a given dielectric volume filling fraction f (Fig. 1a). As described in Supplementary Sect. 1.5, for each wavelength, we compute the scattering mean free path ℓ_s directly from the rate of attenuation of co-polarized field with depth. This, together with the effective wavenumber $k_{\text{eff}} = n_{\text{eff}}(2\pi/\lambda)$, gives the Ioffe–Regel parameter (Fig. 1c). It features a minimum at around $\lambda = 650$ nm and the smallest value of $k_{\text{eff}}\ell_s \simeq\approx 0.9$ is reached at $f = 38\%$. We also compute the transport mean free path ℓ_t from the continuous wave (CW) transmittance of an optically thick slab with thickness $L \gg \ell_t$ (Supplementary Sect. 1.7). In Fig. 1d, $k_{\text{eff}}\ell_t$ also exhibits a dip in the same wavelength range as $k_{\text{eff}}\ell_s$, but the smallest $k_{\text{eff}}\ell_t$ is found at lower f of 18–29%, as the dependent scattering sets in at higher f. In search for AL in this wavelength range, we numerically simulate the propagation of a narrowband Gaussian pulse centred at $\lambda_0 = 650$ nm with planar wavefront and compute the transmittance through the slab $T(t)$ as a function of arrival time t. The diffusive propagation time τ_D approximately corresponds to the arrival time of the peak in Fig. 1e. At $t \gg \tau_D$, the decay of the transmitted flux is exponential over at least 12 orders of magnitude, as expected for purely diffusive systems[46]. The rate of this exponential decay is $1/\tau_D$, which is directly related[46] to the smallest diffusion coefficient within the spectral range of the excitation pulse (Supplementary Sect. 1.8). In Fig. 1f, the dependence of this diffusion coefficient D on the dielectric filling fraction f exhibits a minimum at $f \approx 30\%$. Figure 1e (inset) shows that the further increase of the slab thickness does not lead to any deviation from diffusive transport. Furthermore, the diffusive behaviour persists in the numerical simulation with increased spatio-temporal resolution (Supplementary Sect. 1). At $t \gg \tau_D$, the spatial intensity distribution inside the system features a depth profile (averaged over cross-section) equal to that of the first eigenmode of the diffusion equation (Fig. 1b). We therefore rule out a possibility of AL in uncorrelated ensembles of dielectric spheres with $n = 3.5$.

At microwave frequencies, the refractive index may be even higher than $n = 3.5$. We therefore, perform numerical simulation of a 3D slab of dielectric spheres with $n = 10$. The main results are summarized here, and details are presented in Supplementary Sect. 2. A large scattering cross-section $\sigma_s(\lambda)$ of a single sphere near the first Mie resonance

https://doi.org/10.1038/s41567-023-02091-7

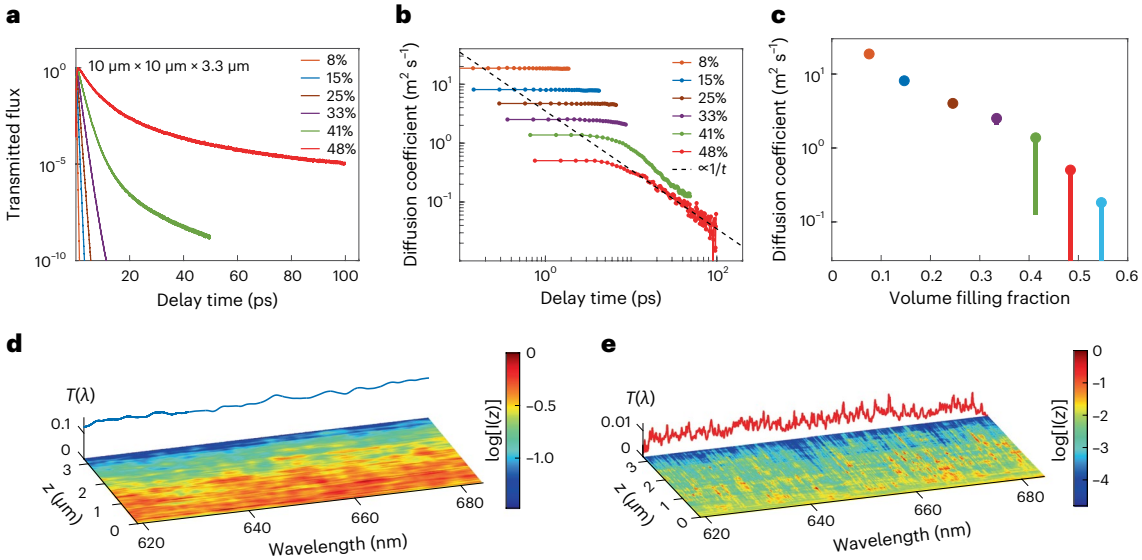

Fig. 2 | AL of light in 3D disordered PEC. a, The transmittance $T(t)$ of an optical pulse through a 3D slab (10 μm × 10 μm × 3.3 μm) of randomly packed PEC spheres with radius $r = 50$ nm and volume filling fraction f from 8% to 48%. **b**, The time-resolved diffusion coefficient $D(t)$ extracted from the decay rate of $T(t)$ in **a**, decreasing with time as $1/t$ at high f. **c**, The short-time D (dots) and the interval of variation of D with time (bars) at different f values. **d**,**e**, The CW transmittance spectrum $T(\lambda)$ in diffusive (**d**, $f = 15\%$, blue line) and localized (**e**, $f = 48\%$, red line) PEC slabs. Colour map: The depth profile of the average intensity $\langle I(x, y_0, z; \lambda)\rangle_x$ inside the slab at different wavelengths, highlighting the localized and necklace-like states for $f = 48\%$.

leads to strong dependent scattering even at small filling fractions. We find the Ioffe–Regel parameter $k_{\text{eff}}\ell_s \gtrsim 1$ despite the very large refractive index difference. This is attributed to dependent scattering that becomes appreciable even at relatively low dielectric filling fraction f. The numerically calculated $T(t)$ for $L/\ell_t \gg 1$ does not exhibit any deviation from diffusive transport: at $t \gg \tau_D$, the decay of transmittance is still exponential over approximately ten orders of magnitude. In addition, scaling of CW transmittance with the inverse slab thickness $1/L$ remains linear for all f, as expected for diffusion (Supplementary Sect. 2). We therefore conclude that AL does not occur in random ensembles of dielectric spheres, thus closing the debate about the possibility of light localization in white paint[8,23].

Previous studies[26,27] suggest that absence of AL for EM waves may be due to longitudinal waves that exist in a heterogeneous dielectric medium, where the transversality condition $\nabla\cdot\mathbf{E}(\mathbf{r}) = 0$ for the electric field $\mathbf{E}(\mathbf{r})$ does not follow from Gauss's law $\nabla\cdot[\epsilon(\mathbf{r})\mathbf{E}(\mathbf{r})] = 0$ because of the position dependence of $\epsilon(\mathbf{r})$. Here, we propose to suppress the contribution of longitudinal waves to optical transport and realize AL of EM waves by using perfectly conducting spheres as scatterers. The Poynting vector is parallel to the surface of a perfect electric conductor (PEC)[47], and EM energy flows around a PEC particle without coupling to longitudinal surface modes. The volume of PEC spheres is simply excluded from the free space and becomes unavailable for light. Thus, at high PEC volume fraction, light propagates in a random network of irregular air cavities and waveguides formed by the overlapping PEC spheres, akin to the original proposal of Anderson[8].

Similarly to the dielectric systems above, we simulate a 3D slab composed of randomly packed, overlapping PEC spheres of radius $r = 50$ nm in air. Figure 2 shows the results of simulating an optical pulse propagating through 10 μm × 10 μm × 3.3 μm slabs of various PEC volume fractions f. $T(t)$ displays non-exponential tails at high $f = 41\%$ or 48% in Fig. 2a. From the decay rate obtained via a sliding-window fit, we extract a time-dependent diffusion coefficient $D(t)$ (Fig. 2b), which shows a power-law decay with time, as predicted by the self-consistent theory of localization[48]. The non-exponential decay of $T(t)$ and the time dependence of D are the signatures of AL[13,48]. In contrast, at lower PEC fractions of $f = 8\%$ or 15%, D remains constant in time. Figure 2c reveals a transition from time-invariant D to time-dependent $D(t)$ at around $f = 33\%$, where $D(t)$ starts deviating from a constant. Using a Fourier transform, we compute the spectrally resolved transmittance $T(\lambda)$. Figure 2d,e contrasts the $T(\lambda)$ of diffusive and localized systems. The former features smooth, gradual variations with λ due to broad overlapping resonances, whereas the latter exhibits strong resonant structures consistent with the average mode spacing exceeding the linewidth of individual modes, in accordance with the Thouless criterion of localization, as the spectral narrowing of modes is intimately related to their spatial confinement[3,9,49]. The colour maps in Fig. 2d,e show the spatial intensity distributions inside the systems, $\langle I(x, y_0, z; \lambda)\rangle_x$, averaged over x at a cross-section $y = y_0$. These two-dimensional maps contrast slow variation with z and λ in the diffusive system (Fig. 2d) to the sharp features due to spatially confined modes in the localized system (Fig. 2e). Furthermore, there exist 'necklace' states with multiple spatially separated intensity maxima, originally predicted for electrons in metals[50].

Insight into the mechanism behind AL in the random ensemble of PEC spheres can be gained from the wavelength dependence of the Ioffe–Regel parameter $k\ell_s$ (Supplementary Sects. 1.5 and 3). We compute it using a procedure similar to that applied in dielectrics. Even at the volume fraction of $f = 8\%$, ℓ_s is well below the prediction of the independent scattering approximation (ISA), owing to scattering resonances formed by two or more neighbouring PEC spheres (Supplementary Fig. S10). As shown in Fig. 3a, ℓ_s becomes essentially independent of wavelength in the range of size parameter kr of PEC spheres. Consequently, the Ioffe–Regel parameter acquires $1/\lambda$ dependence (Fig. 3b). It drops below the value of unity within the excitation pulse bandwidth $\lambda \approx 650 \pm 45$ nm for f between 25% and 33%, in agreement with Fig. 2. We further conduct a finite-size scaling study, after computing the dependence of the CW transmittance T on the slab thickness L (Supplementary Sect. 1.9). Figure 3c shows the logarithmic derivative $\mathrm{d}\log(T)/\mathrm{d}\log(L)$ as a function of $k\ell_s$. In the diffusive regime, Ohm's law $T \propto 1/L$ is expected, leading to a scaling power of −1, as indeed confirmed for $k\ell_s > 1$. Around $k\ell_s \approx 1$, we see a departure from $1/L$ scaling of transmittance. The scaling theory of localization predicts a single-parameter scaling of the dimensionless conductance $g = TN$ (refs. 51,52.). By estimating the number

https://doi.org/10.1038/s41567-023-02091-7

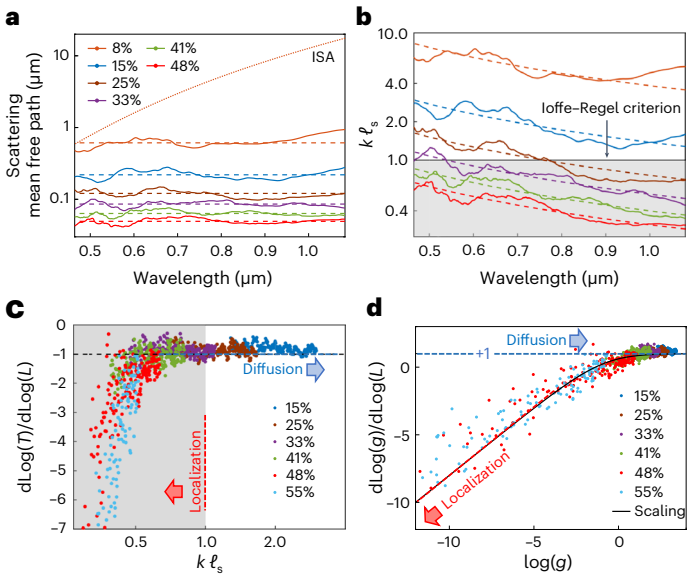

Fig. 3 | The transition from diffusion to AL in 3D disordered PEC. a, The scattering mean free path ℓ_s for PEC volume filling fraction f from 8% to 48%. ℓ_s is nearly flat (dashed lines) over a broad spectral range. **b**, The spectral dependence of the Ioffe–Regel parameter $k\ell_s$, exhibiting $1/\lambda$ dependence (dashed lines). **c**, The scaling of the CW transmittance T with the slab thickness L versus the Ioffe–Regel parameter $k\ell_s$, revealing a diffusion–localization transition at $k\ell_s \approx 1$. The dashed black line denotes diffusive scaling $T \propto L^{-1}$. The dashed red line marks $k\ell_s = 1$. The $k\ell_s < 1$ regime is highlighted as a shaded area in **b** and **c**. **d**, The single-parameter scaling of the dimensionless conductance g for the diffusion–localization transition (solid black line), in agreement with numerical data for six PEC filling fractions. Blue and red dashed lines denote diffusive and localized scalings $g \propto L$ and $g \propto \exp(-L/\xi)$, respectively, where ξ is the localization length.

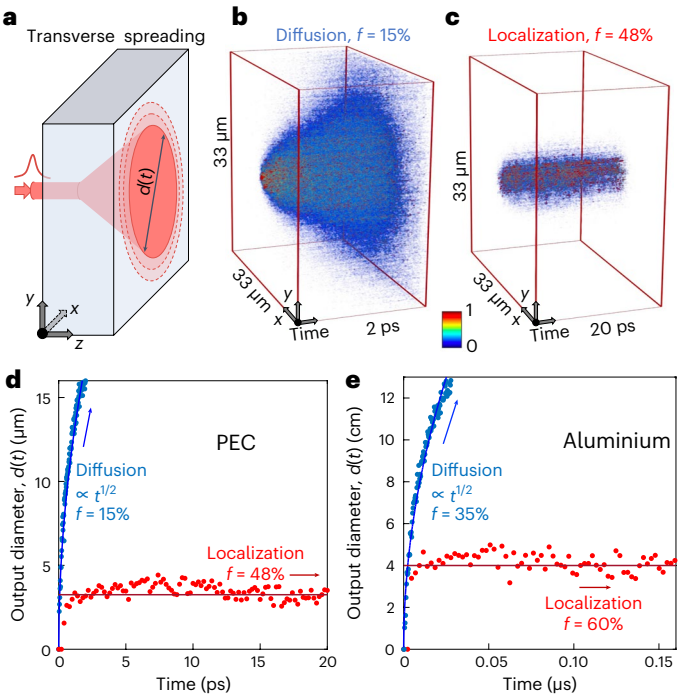

Fig. 4 | Arrest of transverse spreading of transmitted beam in 3D localized PEC systems. a, Schematic of transverse spreading of a tightly focused pulse propagating through a diffusive slab of cross-section 33 μm × 33 μm and thickness $L = 3.3$ μm. **b**, The 2D intensity distribution at the output surface (normalized to the maximum, see colour bar) for different delay times, showing the lateral expansion of the beam in the diffusive slab with PEC filling fraction of $f = 15\%$. **c**, The absence of transverse spreading for $f = 48\%$, owing to AL. **d**, The lateral diameter of the transmitted beam $d(t)$ increases as $\sqrt{t}$ (blue line) in the diffusive slab (blue dots) but saturates to a constant value (red line) in the localized slab (red dots). **e**, The same as **d** but for a slab ($L = 6$ cm) of aluminium spheres ($r = 0.28$ cm, $f = 35\%$ and 60%) with a realistic conductivity value of $\sigma_0 = 3.8 \times 10^4\ \Omega^{-1}\,\mathrm{m}^{-1}$ at a microwave frequency of approximately 20 GHz.

of transverse modes as $N = 2\pi(L/\lambda)^2(1-f)^{2/3}$ for $L \times L$ area of the slab, we compute g and $\beta(g) \equiv \mathrm{d}\log(g)/\mathrm{d}\log(L)$. Figure 3d shows good agreement between the numerical data and the model function $\beta(g) = 2 - (1+g)\log(1+g^{-1})$(ref. 52). In diffusive regime $g > 1$, $\beta(g) \to 1$. Meanwhile, in the localized regime $g < 1$, $\beta(g) \propto \log(g)$. The latter is a manifestation of the negative exponential scaling of g with L in the regime of AL.

To obtain the ultimate confirmation of AL of light in PEC composites, we simulate the dynamics of the transverse spreading of a tightly focused pulse—a measurement that has been widely adopted in localization experiments[13,33,53]. A pulse centred at $\lambda = 650$ nm with a bandwidth of 90 nm is focused to a small spot of area approximately 0.5 μm^2 at the front surface of a wide 3D slab of dimensions 33 μm × 33 μm × 3.3 μm (Fig. 4a). We compute the transverse extent of the intensity distribution $I(x, y, z = L; t)$ at the back surface of the slab. For a diffusive PEC slab with $f = 15\%$, we detect a rapid transverse spreading of light with time in Fig. 4b, which approaches the lateral boundary of the slab within approximately 2 ps. In sharp contrast, in the localized system in Fig. 4c ($f = 48\%$), the transmitted intensity profile remains transversely confined even after 20 ps. This time corresponds to a free space propagation of 6 mm, which is approximately 2,000 times longer than the actual thickness of the slab. Figure 4d quantifies this time evolution with the output beam diameter $d(t) = 2[\mathrm{PR}(t)/\pi]^{1/2}$, where $\mathrm{PR}(t) = [\iint I(x, y, L; t)\mathrm{d}x\,\mathrm{d}y]^2/\iint I(x, y, L; t)^2\mathrm{d}x\,\mathrm{d}y$ is the intensity participation ratio. For a diffusive slab, $d(t) \propto t^{1/2}$, while in the localized regime, $d(t)$ saturates at a value on the order of the slab thickness L. Such an arrest of the transverse spreading in the localized PEC systems persists with increased spatio-temporal resolution of the numerical simulation (Supplementary Sect. 1.3). Further evidence of AL includes non-linear decaying depth profile and strong non-Gaussian fluctuations of intensity inside the system (Supplementary Sect. 4.2). We also confirm our results by repeating calculations for 3D slabs of PEC spheres with larger radius $r = 100$ nm, obtaining similar scaling behaviour (Supplementary Sect. 4.2) as in Fig. 3c,d.

The striking difference between light propagation in dense random ensembles of dielectric and PEC spheres cannot be accounted for by the Ioffe–Regel parameter as both reach $k_{\mathrm{eff}}\ell_s \approx 1$ for similar values of the size parameter kr (Figs. 1c and 3b). AL in 3D PEC composites with uncorrelated disorder reveals a localization mechanism that is unique to metal. In contrast to a dielectric system where light propagates everywhere (both inside and outside the scatterers), the propagation is restricted to the voids between scatterers in the PEC system. This makes AL inevitable when the wavelength becomes larger than the typical width of free-space channels between voids and light can hardly 'squeeze' through the latter to propagate from one void to another. This qualitative picture correctly predicts the increase of the critical volume fraction f for localization with the scatterer size r (Supplementary Sect. 3).

Finally, we test AL in real-metal aggregates. In the microwave spectral region, the skin depth of crystalline metals such as silver, aluminium and copper is several orders of magnitude shorter than the wavelength λ and the scatterer size r in the regime of $kr \approx 1$. Since the microwave barely penetrates into the metallic scatterers, our simulation results are almost identical to those for PEC. To account for the imperfections due to polycrystallinity, surface defects, oxide layers, etc., we lower the metal conductivity to match the experimentally measured

absorption rate in aggregates of aluminium spheres[29]. Simulations unambiguously show the arrest of transverse spreading of a focused pulse (Fig. 4e), revealing AL in 3D random aggregates of aluminium spheres. Additional evidence of AL is presented in Supplementary Sect. 4. Moreover, even at optical frequencies, where realistic metals deviate notably from PEC, the arrest of transverse spreading persists in 3D silver nanocomposites (Supplementary Sect. 5). Possible light localization in 3D nanoporous metals will have a profound impact on their applications in photo-catalysis, optical sensing, and energy conversion and storage.

In summary, our large-scale microscopic simulations of EM wave propagation in 3D uncorrelated random ensembles of particles show no signs of AL for dielectric particles with refractive indices $n = 3.5–10$. This explains multiple failed attempts of experimental observation of AL of light in 3D dielectric systems over the last three decades[22,23,31–33]. At the same time, we report the first numerical evidence of EM wave localization in random ensembles of metallic particles over a broad spectral range. Localization is confirmed by eight criteria: the Ioffe–Regel criterion, the Thouless criterion, non-exponential decay of transmittance under pulsed excitation, vanishing of the diffusion coefficient, existence of spatially localized states, scaling of conductance, arrest of the transverse spreading of a narrow beam and enhanced non-Gaussian fluctuations of intensity. Our study calls for renewed experimental efforts to be directed at low-loss metallic random systems[29]. In Supplementary Sect. 5.1, we propose a realistic microwave experiment that avoids experimental pitfalls and provides a tell-tale sign of AL.

Online content

Any methods, additional references, Nature Portfolio reporting summaries, source data, extended data, supplementary information, acknowledgements, peer review information; details of author contributions and competing interests; and statements of data and code availability are available at https://doi.org/10.1038/s41567-023-02091-7.

References

1. Anderson, P. W. Absence of diffusion in certain random lattices. *Phys. Rev.* **109**, 1492–1505 (1958).
2. Mott, N. Electrons in disordered structures. *Adv. Phys.* **16**, 49–144 (1967).
3. Kramer, B. & MacKinnon, A. Localization: theory and experiment. *Rep. Prog. Phys.* **56**, 1469–1564 (1993).
4. Imada, M., Fujimori, A. & Tokura, Y. Metal–insulator transitions. *Rev. Mod. Phys.* **70**, 1039–1263 (1998).
5. Billy, J. et al. Direct observation of Anderson localization of matter waves in a controlled disorder. *Nature* **453**, 891–894 (2008).
6. Jendrzejewski, F. et al. Three-dimensional localization of ultracold atoms in an optical disordered potential. *Nat. Phys.* **8**, 398–403 (2012).
7. John, S. Electromagnetic absorption in a disordered medium near a photon mobility edge. *Phys. Rev. Lett.* **53**, 2169–2172 (1984).
8. Anderson, P. W. The question of classical localization. A theory of white paint? *Philos. Mag. B* **52**, 505–509 (1985).
9. Chabanov, A. A., Stoytchev, M. & Genack, A. Z. Statistical signatures of photon localization. *Nature* **404**, 850–853 (2000).
10. Schwartz, T., Bartal, G., Fishman, S. & Segev, M. Transport and Anderson localization in disordered two-dimensional photonic lattices. *Nature* **446**, 52–55 (2007).
11. Segev, M., Silberberg, Y. & Christodoulides, D. N. Anderson localization of light. *Nat. Photonics* **7**, 197–204 (2013).
12. Kirkpatrick, T. R. Localization of acoustic waves. *Phys. Rev. B* **31**, 5746–5755 (1985).
13. Hu, H., Strybulevych, A., Page, J. H., Skipetrov, S. E. & van Tiggelen, B. A. Localization of ultrasound in a three-dimensional elastic network. *Nat. Phys.* **4**, 945–948 (2008).
14. Guazzelli, E., Guyon, E. & Souillard, B. On the localization of shallow water waves by random bottom. *J. Phys. Lett.* **44**, 837–841 (1983).
15. Sheng, P., White, B., Zhang, Z. Q. & Papanicolaou, G. in *Scattering and Localization of Classical Waves in Random Media, Directions in Condensed Matter Physics* (ed. Sheng, P.) 563–619 (World Scientific, 1990).
16. Rothstein, I. Z. Gravitational Anderson localization. *Phys. Rev. Lett.* **110**, 011601 (2013).
17. John, S. Localization of light. *Phys. Today* **44**, 32–40 (1991).
18. Sheng, P. *Introduction to Wave Scattering, Localization and Mesoscopic Phenomena* (Springer, 2006).
19. Lagendijk, A., van Tiggelen, B. & Wiersma, D. S. Fifty years of Anderson localization. *Phys. Today* **62**, 24–29 (2009).
20. Ioffe, A. F. & Regel, A. R. Non-crystalline, amorphous, and liquid electronic semiconductors. *Prog. Semicond.* **4**, 237–291 (1960).
21. Haberko, J., Froufe-Perez, L. S. & Scheffold, F. Transition from light diffusion to localization in three-dimensional amorphous dielectric networks near the band edge. *Nat. Commun.* **11**, 4867 (2020).
22. van der Beek, T., Barthelemy, P., Johnson, P. M., Wiersma, D. S. & Lagendijk, A. Light transport through disordered layers of dense gallium arsenide submicron particles. *Phys. Rev. B* **85**, 115401 (2012).
23. Sperling, T. et al. Can 3D light localization be reached in 'white paint'? *N. J. Phys.* **18**, 013039 (2016).
24. Lahini, Y. et al. Anderson localization and nonlinearity in one-dimensional disordered photonic lattices. *Phys. Rev. Lett.* **100**, 013906 (2008).
25. Skipetrov, S. E. & Page, J. H. Red light for Anderson localization. *N. J. Phys.* **18**, 021001 (2016).
26. Skipetrov, S. E. & Sokolov, I. M. Absence of Anderson localization of light in a random ensemble of point scatterers. *Phys. Rev. Lett.* **112**, 023905 (2014).
27. van Tiggelen, B. A. & Skipetrov, S. E. Longitudinal modes in diffusion and localization of light. *Phys. Rev. B* **103**, 174204 (2021).
28. Cobus, L. A., Maret, G. & Aubry, A. Crossover from renormalized to conventional diffusion near the three-dimensional Anderson localization transition for light. *Phys. Rev. B* **106**, 014208 (2022).
29. Genack, A. Z. & Garcia, N. Observation of photon localization in a three-dimensional disordered system. *Phys. Rev. Lett.* **66**, 2064–2067 (1991).
30. Watson Jr, G., Fleury, P. & McCall, S. Searching for photon localization in the time domain. *Phys. Rev. Lett.* **58**, 945 (1987).
31. Wiersma, D. S., Bartolini, P., Lagendijk, A. & Righini, R. Localization of light in a disordered medium. *Nature* **390**, 671–673 (1997).
32. Störzer, M., Gross, P., Aegerter, C. M. & Maret, G. Observation of the critical regime near Anderson localization of light. *Phys. Rev. Lett.* **96**, 063904 (2006).
33. Sperling, T., Bührer, W., Aegerter, C. M. & Maret, G. Direct determination of the transition to localization of light in three dimensions. *Nat. Photonics* **7**, 48–52 (2013).
34. Scheffold, F., Lenke, R., Tweer, R. & Maret, G. Localization or classical diffusion of light? *Nature* **398**, 206–207 (1999).
35. Wiersma, D. S., Rivas, J. G., Bartolini, P., Lagendijk, A. & Righini, R. Reply: Localization or classical diffusion of light? *Nature* **398**, 207–207 (1999).
36. Scheffold, F. & Wiersma, D. Inelastic scattering puts in question recent claims of Anderson localization of light. *Nat. Photonics* **7**, 934 (2013).
37. Gentilini, S., Fratalocchi, A., Angelani, L., Ruocco, G. & Conti, C. Ultrashort pulse propagation and the Anderson localization. *Opt. Lett.* **34**, 130–132 (2009).

38. Pattelli, L., Egel, A., Lemmer, U. & Wiersma, D. S. Role of packing density and spatial correlations in strongly scattering 3D systems. *Optica* **5**, 1037–1045 (2018).
39. *Flexcompute Inc.* https://flexcompute.com (2021).
40. Hughes, T. W., Minkov, M., Liu, V., Yu, Z. & Fan, S. A perspective on the pathway toward full wave simulation of large area metalenses. *Appl. Phys. Lett.* **119**, 150502 (2021).
41. Lu, L., Joannopoulos, J. D. & Soljacic, M. Topological photonics. *Nat. Photonics* **8**, 821–829 (2014).
42. Stützer, S. et al. Photonic topological Anderson insulators. *Nature* **560**, 461–465 (2018).
43. Sapienza, L. et al. Cavity quantum electrodynamics with Anderson-localized modes. *Science* **327**, 1352–1355 (2010).
44. Wiersma, D. S. Random quantum networks. *Science* **327**, 1333–1334 (2010).
45. Cao, H. & Eliezer, Y. Harnessing disorder for photonic device applications. *Appl. Phys. Rev.* **9**, 011309 (2022).
46. Akkermans, E. & Montambaux, G. *Mesoscopic Physics of Electrons and Photons* (Cambridge Univ. Press, 2007).
47. van de Hulst, H. C. *Light Scattering by Small Particles* (Dover, 1981).
48. Skipetrov, S. E. & van Tiggelen, B. A. Dynamics of Anderson localization in open 3D media. *Phys. Rev. Lett.* **96**, 043902 (2006).
49. Thouless, D. J. Electrons in disordered systems and the theory of localization. *Phys. Rep.* **13**, 93–142 (1974).
50. Pendry, J. B. Quasi-extended electron states in strongly disordered systems. *J. Phys. C* **20**, 733–742 (1987).
51. Abrahams, E., Anderson, P. W., Licciardello, D. C. & Ramakrishnan, T. V. Scaling theory of localization: absence of quantum diffusion in two dimensions. *Phys. Rev. Lett.* **42**, 673–676 (1979).
52. Müller, C. A. & Delande, D. In *Ultracold Gases and Quantum Information: Lecture Notes of the Les Houches Summer School in Singapore* (eds. Miniatura, C.) Chapter 9 (Oxford Univ. Press, 2011).
53. Cherroret, N., Skipetrov, S. E. & van Tiggelen, B. A. Transverse confinement of waves in three-dimensional random media. *Phys. Rev. E* **82**, 056603 (2010).

Data availability

Figures reported in this work, containing the source data, are available via download from https://scholarsmine.mst.edu/phys_facwork/2259/. All other data that support the findings of this study are available from the corresponding authors upon reasonable request. Source data are provided with this paper.

Code availability

The simulation project and associated codes can be found at https://www.flexcompute.com/userprojects/anderson-localization-of-electromagnetic-waves-in-three-dimensions. A Tidy3D software license can be requested from Flexcompute Inc to reproduce simulation results.

Acknowledgements

This work is supported by the National Science Foundation under grant nos. DMR-1905442 and DMR-1905465 and the Office of Naval Research (ONR) under grant no. N00014-20-1-2197. We thank S. Fan and B. van Tiggelen for enlightening discussions. A.Y. expresses gratitude to LPMMC (CNRS) for hospitality.

Author contributions

A.Y. performed numerical simulations, analysed the data and compiled all results. S.E.S. conducted theoretical study and guided data interpretation. T.W.H. and M.M. implemented the hardware-accelerated FDTD method and aided in the setup of the numerical simulations. Z.Y. and H.C. initiated this project and supervised the research. A.Y. wrote the first draft, S.E.S. and H.C. revised the content and scope, and T.W.H., M.M. and Z.Y. edited the manuscript. All co-authors discussed and approved the content.

Competing interests

T.W.H., M.M. and Z.Y. have financial interest in Flexcompute Inc., which develops the software Tidy3D used in this work.

Additional information

Supplementary information The online version contains supplementary material available at https://doi.org/10.1038/s41567-023-02091-7.

Correspondence and requests for materials should be addressed to Alexey Yamilov, Zongfu Yu or Hui Cao.

Peer review information *Nature Physics* thanks Luis Froufe-Pérez, Diederik Wiersma and the other, anonymous, reviewer(s) for their contribution to the peer review of this work.